**Decoding urban landscapes: Google Street View and measurement sensitivity**

**Accepted Version**

**(Note: Published in *Computers, Environment and Urban Systems* Vol. 88, 101626.
doi: 10.1016/j.compenvurbsys.2021.101626
The final publication is available at www.sciencedirect.com)**

Jae Hong Kim
Department of Urban Planning and Public Policy
University of California, Irvine
206E Social Ecology I, Irvine, California, USA, 92697
Phone: 1.949.824.0449
Fax: 1.949.824.8566
Email: jaehk6@uci.edu

Sugie Lee
Department of Urban Planning & Engineering
Hanyang University
Email: sugielee@hanyang.ac.kr

John R. Hipp
Department of Criminology, Law and Society and Department of Sociology
University of California, Irvine
Email: hippj@uci.edu

Dong Hwan Ki
Department of Urban Planning & Engineering
Hanyang University
Email: orient1477@naver.com

**Decoding urban landscapes: Google Street View and measurement sensitivity**

**Abstract:** While Google Street View (GSV) has been increasingly available for large-scale examinations of urban landscapes, little is known about how to use this promising data source more cautiously and effectively. Using data for Santa Ana, California, as an example, this study provides an empirical assessment of the sensitivity of GSV-based streetscape measures and their variation patterns. The results show that the measurement outcomes can vary substantially with changes in GSV acquisition parameter settings, specifically spacing and direction. The sensitivity is found to be particularly high for some measurement targets, including humans, objects, and sidewalks. Some of these elements, such as buildings and sidewalks, also show highly correlated patterns of variation indicating their covariance in the mosaic of urban space.

## 1. Introduction

As our cities evolve rapidly over time, so does our analytical environment for urban research. Recent decades, in particular, have seen significant methodological advancements in measuring and analyzing urban landscapes and their variation at a fine scale (which is in part attributable to widespread geographic information system (GIS) applications and continuing development of information technologies, more broadly). New data sources, such as high-resolution satellite imagery, geocoded street views, and social media data, have also been increasingly utilized for this purpose, while Census, local land-use/building inventories, and other traditional sources of information have remained essential.

One particular data source that has gained much popularity is Google Street View (GSV) imagery.[1] Even though some of its drawbacks, especially seasonal and time variability, have been pointed out, the potential of GSV as a valuable source of information has been widely recognized across disciplines. At the same time, increasing efforts have been made to assess the validity and usefulness of GSV, often by comparing what GSV imagery conveys with what we would actually see and feel on the street (see, e.g., Bader et al., 2017; Campbell et al., 2019; Nesse and Airt, 2020). Over the last several years, some researchers have also started to use GSV more actively for large-scale projects by employing API and machine learning technologies

[1] Since its inception in 2007 in some U.S. cities, GSV has expanded its territory to all seven continents to achieve its mission "to organize the world's information and make it universally accessible and useful" (Anguelov et al., 2010, p.32). Although some countries have restricted the production of GSV images, over the last decade it has become available for almost every corner of cities in many countries and contributed significantly to the widespread use of street imagery for a variety of purposes. It has also served as a leading player in the "street-level imagery ecosystem," where new service providers have emerged and transformed the workings of geo-coded imagery data platforms (Leon and Quinn, 2019).

in collecting and processing a massive amount of imagery data (see, e.g., Gebru et al., 2017; Lu et al., 2019; Middel et al., 2019; Yang et al., 2019; Law et al., 2020).

Despite the ongoing efforts, however, many questions remain unanswered regarding how researchers should take advantage of this (seemingly) promising dataset in measuring our cities and their granular fabrics. A particularly important challenge is simply the scale of the data. Using GSV images for a large region can result in a time intensive data acquisition and image analysis process. As a consequence, rather than obtaining every image available in a study area, researchers often choose to collect a smaller sample. Although this does not necessarily introduce biases—depending on how it is done—but it can reduce the reliability of the measures constructed from the data. How large of a problem is this reduced reliability for researchers? And, are some ways better than others for collecting these smaller samples from a study area in empirical studies? For example, how impactful is it to increase the distance between acquired images, or to only extract images from the midpoint of a street segment? Furthermore, do these decisions have varying consequences when capturing different streetscape features, such as buildings, sidewalks, or traffic signs?

Little is known about these questions, and little guidance is available on how one should make decisions regarding gathering and processing street images from GSV and how the resultant GSV-based measures might vary based on the choices made. In this study, we attempt to draw attention to the importance of some key parameters – spacing, directions, and target features – that are determined in the GSV image acquisition/utilization process. In addition, we provide an empirical assessment of the (global) sensitivity – i.e., to what extent urban landscape measures (captured through GSV images) vary depending on the parameters – and (local)

variation patterns – i.e., how the variation changes over space – in order to inform future research.

The remainder of this article is organized as follows. The next section provides a review of existing studies with a focus on how they gathered and processed GSV images for various urban research purposes. Section 3 presents the data and methods used for our empirical assessment of the global and local sensitivity patterns with respect to spacing, directions, and target features. The results are presented in section 4, which is followed by some concluding remarks and discussion.

## 2. Literature Review

### *2.1. Growing popularity of GSV*

While the use of GSV in the academic literature is still in its infancy, an increasing number of researchers have utilized GSV for an expanding range of research topics. The Web of Science (WOS) clearly shows this trend and the wide range of academic disciplines employing GSV (see Figure 1). The upward trend is particularly evident in urban studies, geography, planning, and related fields, as GSV provides a rare opportunity to extract information about urban landscapes with a high level of spatial precision.

<< Insert Figure 1 about here >>

For instance, GSV has been increasingly seen as a useful resource that enables one to measure streetscape greenery precisely and thus to examine the effects of vegetation on residents' well-being more effectively (see e.g., Seiferling et al., 2017; Li et al., 2018; Lu, 2019). Scholars have

also recognized its potential for detecting pedestrians and vehicles to analyze urban travel patterns or even estimate the demographic makeup of neighborhoods (see e.g., Yin et al., 2015; Gebru et al., 2017; Goel et al., 2018). The increasing use of GSV shown in Figure 1 undoubtedly reflects these promises, and there have been efforts to explore new ways of exploiting GSV to better understand how our cities work and evolve over time, as discussed below.

*2.2. GSV and its evolving use in applied research*

Early studies often used GSV imagery to supplement data from other sources for their investigations of some (pre)selected sites/households or gauged the feasibility of GSV-based approaches to measuring urban landscapes. Curtis et al. (2010), for instance, took advantage of GSV as "a proxy for spatial video data" (p.54) to identify patterns of post-Katrina abandonment and recovery at the building level in the Holy Cross neighborhood of New Orleans. Guo (2013) measured levels of on- and off-street parking availability using GSV images (in combination with areal phots and tax lot maps) for a sample of 403 households in the New York city region to examine the relationship between residential parking supply and household car ownership. In their highly-cited study on the pathways of urban neighborhood transformation, Hwang and Sampson (2014) utilized GSV in order to identify and detect distinct signs of gentrification and thus explore the varying trajectories of neighborhood change across 140 census tracts in Chicago. Lee and Talen (2014) examined the potential usefulness of GSV in developing a new GIS-based auditing method for systematic assessment of built environment characteristics, focusing on ten street segments on an arterial road in Phoenix.

While such examinations (with a relatively small sample size which makes it possible to extract the necessary information through a careful inspection of street images) have continued (e.g., He et al., 2017; Egli et al., 2019; Gobster et al., 2020), the literature has also embraced larger-scale applications of GSV in the last several years. The latter studies have typically collected GSV imagery from numerous location points and employed automated image processing techniques which have become more accessible with the rapid development of machine learning technologies (see e.g., Lu et al., 2019; Middle et al., 2019; Nugyen et al., 2019). The merit of these large-scale applications lies in their comprehensive scope and ability to capture the spatial/distributional pattern of interest within an entire city/region or even nationwide.

Gebru et al. (2017) provided a good example of one of the largest-scale applications of GSV imagery in an investigation of urban neighborhoods. The authors used 50 million GSV images drawn from 200 cities in the U.S. to detect auto vehicles and their detailed attributes (e.g., make, model, year) that were assumed to reflect the demographic makeup of the places. Specifically, they developed a unique "census of motor vehicles" (p.13108) through a two-step procedure, consisting of (1) car detection using an object recognition algorithm and (2) car (object) classification into a few thousand vehicle categories using a deep learning technique. Their study demonstrated the value of GSV imagery collected and processed in this big-data-analysis fashion by showing that the vehicle data derived from GSV yielded high accuracy in estimating a range of demographic characteristics parameters. Nugyen et al.'s (2019) study is another notable example of such large-scale applications of GSV imagery. Using over 16 million GSV images gathered from street intersections across the United States, they measured

various characteristics of the built environment and analyzed how the location-specific characteristics were associated with public health outcomes in a comprehensive manner.

This large-scale mode of data mining/processing has proliferated more rapidly in some areas of urban research, particularly those concerning street greenery and its contribution to promoting human physical activities, such as walking and cycling. A growing number of researchers have measured the amount of street greenery at a fine scale using GSV through this approach and explored the implications of greenness from the perspective of urban design/planning and public health. Seiferling et al. (2017), for instance, analyzed over 450,000 GSV images using a multi-step image segmentation method to precisely capture tree presence and distribution in Boston and New York. Li et al. (2018) examined the association between streetscapes and walking activities using tens of thousands of GSV panorama and horizontal static images which were extracted every 100 meters along streets in the city of Boston. Other studies have also used GSV imagery information in a similarly large-scale fashion to analyze the distribution of green spaces in some other places, such as Hong Kong (Lu, 2019; Lu et al., 2019; Yang et al., 2019) and Singapore (Ye et al., 2019). Furthermore, recent studies on solar radiation (or light pollution) have exemplified this tendency of large-scale image acquisition and processing through an automated (and machine learning-based) procedure. These studies have typically used a massive amount of street imagery to measure the sky visibility at numerous location points with varying degrees of street tree canopy and building structure (e.g., Gong et al. 2018; Li and Ratti, 2019; Li et al., 2019; Middle et al, 2019).

### *2.3. A research gap*

In the literature, however, scholars have generally paid limited attention to the importance of street imagery acquisition and processing methods. In carrying out a large-scale GSV application, researchers are faced with a series of decision points that might affect the quality of information gathered quite substantially. Among others, one should determine an appropriate frequency or (distance) spacing scheme to extract GSV images from the study area in an orderly fashion. While using longer intervals (e.g., collecting GSV data from a point for every 100 meters) reduces the burden of data acquisition, it can decrease the ability to precisely capture rapid streetscape transition that may take place in some areas. Equally important is setting up the direction(s) for GSV image collection at each data gathering point. The street view on one side can differ significantly from that of the other side. Also, some streetscape features (e.g., buildings and sidewalks) are more likely to appear in the scene, when the direction is set in a certain manner.

In many urban research settings, the collected street images have to be processed further in a certain way focusing on some specific elements of the urban landscape. In a study on urban green space, for instance, various types of vegetation should be parsed out. When transportation infrastructure (or travel behavior) is of interest, consideration would be given to road surface, sidewalks, vehicles, or even pedestrians in the scene. While the particular elements of interest vary across studies (and this largely depends on the research topic and/or the theories to be tested), researchers should identify an appropriate set of target features that would allow them to measure the urban landscape effectively for their own research purposes. A well-defined set of target features is particularly important when a great deal of street imagery needs to be processed through an automated procedure.

Table 1 summarizes a sample of studies using GSV in such an extensive manner and showing the promise of GSV imagery. As shown in the table, a broad range of data acquisition settings (e.g., 20-meter, 50-meter and 100-meter intervals for spacing) have been employed in utilizing GSV data for applied urban research. It is important to note that some of the studies chose certain parameter settings purposefully and provided a justification for their decision. In other studies, however, the choices can appear somewhat arbitrary with little explanation provided. As briefly mentioned above, longer distance intervals might have reduced reliability for capturing micro-level variation in the built environment if the study area's streetscape changes rapidly over space. Furthermore, the marginal benefit of reducing the size of intervals (and thus collecting more GSV images) may not be the same over all studies, but may actually depend on issues such as the particular features being targeted in the study.

<< Insert Table 1 about here >>

Despite the importance of these GSV acquisition settings, there is a dearth of research that rigorously examines to what extent (and in what ways) the data collection method may influence the urban landscape measures derived from GSV or comparable sources of street imagery information. Little guidance is available for future research that would take advantage of the rich information embedded in GSV extensively. This is an important issue, as whereas in a small-scale study a researcher might simply collect and inspect all images available at every data point, in large-scale studies a more extensive use of street view imagery requires a deliberate process of setting up the data acquisition/processing parameters to capture the constructs of interest effectively, given the time, data storage, and computation issues involved. Our study here attempts to inform future research by assessing how GSV-based streetscape measurement outcomes can be affected by the method used to collect GSV images, specifically

the distance intervals and direction settings. In doing so, this study explores the tradeoffs between various possible strategies that combine different distance intervals and directional settings (e.g., longer intervals with a 360-degree view vs. shorter intervals with a narrower angle in a certain direction) for measuring the streetscape efficiently. Furthermore, explicit attention is paid to how the measurement sensitivity varies by target feature (e.g., buildings vs. vegetation) to support a broad range of research that could be benefited by the informed use of GSV.

## 3. Data and Methods

### *3.1. Study Area*

Our assessment focuses on the City of Santa Ana which is the county seat of Orange County, California. Santa Ana is one of the few cities in the county incorporated in the 19$^{th}$ century (1886), and the city has remained one of the largest jurisdictions in terms of both population (approximately 330,000 in 2019) and physical size (approximately 27.3 square miles) in the county.

While every city is unique in some sense, Santa Ana contains a wide spectrum of development patterns within its boundaries and thus provides a good opportunity to understand the workings of GSV in various urban settings. Both old and new development styles coexist in the city, and parts of the city well represent some common characteristics of small or mid-sized cities which have attracted relatively little attention in previous GSV research. The city also encompasses varying degrees of density, vacancy, and land use mix across neighborhoods. Furthermore, it has various transportation options, ranging from freeways and road arterials to an airport and transit routes/stops, all of which are important elements of American cities.

Figure 2 shows the city's street layout. The city has over 5,000 street segments, totaling approximately 450 miles (724 kilometers) in length.

<< Insert Figure 2 about here >>

*3.2. Data*

For the present assessment, we collected GSV street images for each of the street segments in Santa Ana. Specifically, first, we identified over 30,000 data acquisition points with 20-meter intervals between them and acquired four images (and their metadata) from each point that represent distinct street views in four directions (front, back, left, and right) using the GSV API. All the data points were coded in a way to determine whether they would be selected if an alternative spacing scheme (40m, 60m, 80m, or 100m) were adopted – which is one of the key parameters in our assessment of the measurement sensitivity. Additionally, we identified the midpoint of each segment and repeated the image collection process (again with four directions) at these location points that represent another data acquisition setting one could adopt, as done in Law et al. (2020).

It needs to be noted that in this data collection process, we applied a 10-meter buffer to each street intersection and excluded areas near intersections, since the street images there tend to capture the physical environment of more than a single segment. Consideration was also given to the time point at which the images were taken, and we used GSV images taken between April 2017 and March 2020 to have observations for as many segments as possible after a careful review of the GSV metadata collected. Although this time window is wider than ideal, the images on a single street segment were taken at the same time in most cases. About 5% of the

street segments in the city had images taken on different days at the segment level, and we excluded these street segments from our analysis, explained in detail below.[2]

Then, the collected GSV images were processed through semantic segmentation that allowed us to classify detailed image components (e.g., buildings, roads, vegetation). More specifically, among several semantic segmentation techniques available, we employed the Deeplabv3+ model (Chen et al., 2018) that extended Deeplabv3 (Chen et al., 2017) and demonstrated strong performance on multiple datasets (Chen et al., 2018). Given its superior performance, the Deeplabv3+ model has increasingly been adopted for image processing (see, e.g., Barbierato et al., 2020; Wang & Vermeulen, 2020), and we used the model pre-trained using the Cityscapes dataset (Cordts et al., 2016) that contained a comprehensive set of daytime urban scene images, enabling researchers to make their models recognize detailed streetscape elements effectively, as others would do. This model allowed us to classify all the street view image pixels into one of the following nine categories representing a range of target features of (potential) interest: buildings (including fences and walls), humans, objects (poles, traffic lights, and traffic signs), roads, sidewalks, sky, terrain, vegetation, and vehicles (all types of vehicles, such as cars, trucks, and motorcycles).

We applied the model to all the GSV images and then calculated the proportion of each of the nine categories in each image for our assessment of the sensitivity of GSV-based streetscape measures. This replicates what urban researchers have done, often focusing on one or few target features. Figure 3 illustrates this process using some examples.

[2] Although we excluded these street segments from our analysis, one could wonder how much of an issue such segments might cause for analyses. We assessed this for our study area and found that the measures constructed based on all street segments (including those with images from different years) yielded extremely similar results to those presented in the study. This is unsurprising given that: (1) these potentially problematic segments only include a small fraction of the observations and (2) the built environment tends to change slowly over time.

<< Insert Figure 3 about here >>

*3.3. Methods*

As briefly mentioned above, in this study, the focus is on three key parameters to be determined in gathering and processing GSV imagery: spacing (*s*), directions (*d*), and target features (*f*). In a very large-scale project, researchers may wish to collect and analyze images in a consistent and efficient fashion, and do so by restricting one or more of these three parameters. We assessed both the (global) sensitivity – i.e., to what extent GSV measures vary depending on the three parameters – and (local) variation patterns – i.e., where (or under what circumstances) the degree of variation tends to be larger. To do this, our assessment considered 6 spacing options, 7 directional settings, and 9 target features, as listed below.[3]

- *s*: 20m, 40m, 60m, 80m, 100m intervals, and midpoints
- *d*: front, back, left, right, front+back (FB), left+right (LR), and all four directions (FBLR)
- *f*: buildings, humans, objects, roads, sidewalks, sky, terrain, vegetation, and vehicles

This assessment framework allowed us to derive GSV measures with 42 (6×7) data acquisition parameter settings (which can be compared with each other) for each of the nine target features. Given the large number of measurement outcomes to be handled, we used a straightforward approach to assessing the measurement sensitivity and its variation patterns. Specifically, we examined the global sensitivity based upon (Pearson) correlations between the GSV measures

[3] This range of distance intervals (20m to 100m) covers the spacing parameter settings used by most previous studies, and the constant interval increase (by 20m at a time) intends to compare the results in a systematic fashion. The nine target features considered represent an array of streetscape elements that have been examined by various studies.

generated from two different parameter settings for each target feature. This can be expressed as:

$$correlation[p^{f(h)}_{s(i),d(j)}, p^{f(h)}_{s(k),d(l)}] \qquad \text{with } (i,j) \neq (k,l)$$

where $p^{f(h)}_{s(i),d(j)}$ indicates the average proportion of a target feature (*h*-th type) in the GSV images collected from each street segment with a spacing and directional setting, denoted by *s(i)* and *d(j)* respectively. To be more specific, for a 200-meter-long street segment for which we had 10 GSV acquisition points with 20-meter intervals, we combined the information from up to 40 GSV images (20m-FBLR) to compute the average proportion of each target feature on that segment. Based on alternative parameter settings, we derived the proportion with a smaller number of images (e.g., 10 images for 20m-left, 8 images for 100m-FBLR) for the same street segment. As noted above, there are 42 *s-d* combinations, and this means a total of 861 correlations (41+40+ … +2+1) that can be used to reveal the overall patterns of global sensitivity for each target feature. In order to interpret the results effectively, we regarded GSV measures derived from 20m-FBLR ($p^{f(h)}_{20m,FBLR}$) as a "baseline" (as this approach used the largest number of images) and focused on the comparison of other strategies and the baseline, while we checked the correlation patterns for the remaining pairs (e.g., 20m-left vs. 20m-right) and will discuss such results briefly in the next section.

For the assessment of local variation patterns, we used multivariate regression models that were designed to detect the associations between the degree of variability on each street segment (dependent variable) and the segment's unique characteristics (covariates). Here, using $p^{f(h)}_{20m,FBLR}$ as the baseline as mentioned above, we computed the deviation from this baseline for each of the alternative 41 *s-d* combinations to construct the dependent variable. To be more precise, our dependent variable is formulated as

$$abs[z(p^{f(h)}_{s(i),d(j)}) - z(p^{f(h)}_{20m,FBLR})] \quad \text{with } (i,j) \neq (20m, FBLR)$$

indicating the absolute magnitude of the deviation from the baseline (in terms of the standardized z score) on each street segment, when an alternative spacing and directional setting (*i*,*j*) was adopted to measure the streetscape. For the covariates, we used the street segment length (given that it likely impacts the ability to measure a street with fewer images), as well as the $z(p^{f(h)}_{20m,FBLR})$ values for all but one target feature category (to avoid singularity). These target feature categories collectively represent the detailed street attributes and their locational characteristics (e.g., highly developed areas vs. low-density locations).

With this set-up, we estimated the regression models in this standardized fashion for all combinations of the 9 target features and 41 alternative data acquisition parameter settings (42 minus the baseline), yielding a total of 369 sets of model estimation results. For these model estimations (as well as the correlation calculations for the global sensitivity analysis), we used the GSV images drawn from 1,908 street segments in Santa Ana for which at least one observation for all the six spacing options was available. Although a large number of short (< 100 meter) segments were excluded, this approach allowed us to examine the global and local sensitivity patterns in a consistent manner. The 1,908 segments used account for over 55% of the total length of the street networks in the city.

## 4. Results

### *4.1. Overall global sensitivity patterns*

Any modification of the GSV acquisition parameters – spacing and directional settings – results in changes in the street-level measurement outcomes, and we quantified and assessed this sensitivity in terms of correlations, as described in the previous section. With respect to the first parameter of interest (spacing), in general, the correlation value declined more substantially (indicating larger changes in the measurement outcomes), as the spacing gap widened. When all four directions (FBLR) were taken into account, the 20m-40m correlations ranged from 0.837 (humans) to 0.984 (buildings) with a mean of 0.951, indicating little variation due to the relatively longer intervals (Table 2). However, as we subsequently had a larger distance between acquisition points going down these rows in Table 2, the overall mean declined gradually and was 0.805 for 20m-100m pairs (See also Appendix A for the analysis results with other directional settings). The midpoint approach (having the smallest number of data points because it used only one data acquisition point per segment) showed an even lower correlation (with a mean of 0.777 across nine target feature categories) implying even more variation in the GSV measures.

<< Insert Table 2 about here >>

A similar pattern of correlation decline was detected when the number of observations for each street segment decreased due to changes in directional settings – the second parameter of interest in this study (Table 3). Specifically, with 20-meter intervals, the correlation between all four directions and left+right (FBLR vs. LR) ranged from 0.901 (sidewalks) to 0.991 (terrain) with a mean of 0.960 across nine target features (the second row in Table 3). The mean correlation value was lower, 0.928, for front+back (FB) and further declined for the four single-directional settings in the following order: 0.880 (back), 0.867 (front), 0.760 (left), and 0.750 (right). Thus, it appears that the least reliable strategy would be to only collect images from a

single side of the road (either left or right), a point to which we will return (See also Appendix B for the analysis results with other spacing schemes).

<< Insert Table 3 about here >>

It should be noted that the correlation decline was even larger when both spacing and directions were altered in a way that required us to use a smaller number of GSV images for each segment (i.e., sparser spacing combined with one or two directions). To be more specific, as shown in Appendix B, while the mean correlation between all directions and front+back (FBLR vs. FB) was 0.928 with 20-meter intervals, the mean decreased to 0.897 (40m), 0.865 (60m), 0.852 (80m), 0.836 (100m), and 0.821 (midpoints); and this pattern holds for other directional settings. Similarly, the correlations between two spacing options tended to be lower, when only one or two directions were used in the image acquisition process. For example, as presented in Appendix A, the mean 20m-40m correlation, which was 0.951 for all four directions as noted above, went down to 0.911 (left+right), 0.913 (front), 0.917 (back), 0.900 (left), and 0.898 (right).

This finding suggests that tradeoffs exist between spacing and directional settings, if one seeks to limit the number of GSV images to be collected/processed. In other words, one could mitigate the variability that arises due to sparser spacing to some extent, using all four directions (though the directional setting should reflect each study's research objectives) or vice versa. In Appendix C, we compare each possible way of collecting GSV data to the baseline of all four images every 20 meters. We can think about these as tradeoffs in which the number of collected images is a "cost." With this in mind, we find that collecting 4 images with sparser spacing (every 40 meters) shows a 6.4% reduction in reliability compared to the baseline, whereas there is a bit more loss when collecting images every 20 meters but just left and right (9.0% reliability

reduction), even though these different strategies imply similar numbers of images. As demonstrated in the Appendix, the sensitivity varies across target features – an important point which will be discussed in detail in the following subsection.

Another notable finding is that the left and right sides showed sharp differences in terms of GSV-based streetscape measures. Unlike selecting either front or back images, which tended to be relatively similar, selecting either left or right images exhibited sharply lower correlation values (Table 4). For many target features, the left-right correlations were lower not only than those for front-back but also than other pairs, such as front-left, front-right, back-left, and back-right, highlighting the asymmetry of urban streetscapes in this sense. In particular, sidewalks showed negative correlation values for left-right pairs. These results provide a caution that directional choices should be made carefully in using GSV imagery.

<< Insert Table 4 about here >>

*4.2. Sensitivity by target feature*

The sensitivity of the measurement outcomes varies considerably across target features. As seen in Table 2, the correlation values tended to be higher for more common features that accounted for a larger proportion of the scene, such as sky and vegetation, which make up 34% and 22% of the GSV image pixels, respectively, on average in our sample (see bottom of Table 2 for the proportions of all nine features). In contrast, humans and objects comprised a small proportion of the images (0.1% and 0.4%, respectively) and generally had much lower correlations (i.e., are more sensitive). There are, however, some notable exceptions – for instance, terrain showed relatively higher correlations than vehicles, whereas it accounted for a smaller proportion of the scene (2.4%, cf. vehicles: 4.3%) on average. This finding may be attributed to the fact that the

amount of terrain does not vary significantly on a single street segment. On the contrary, the appearance of vehicles can fluctuate even in a single street block, resulting in more sensitivity at the street segment level.

It is important to note that some target features presented distinct patterns of sensitivity with respect to spacing vs. directional setting changes. For example, humans showed the highest variability in response to spacing modifications, indicated by the rapid correlation decline with sparser spacing options in Table 2 (from 0.837 at 40 meters to 0.539 at 100 meters, and just 0.488 using the midpoints), and this finding may be attributable to their mobility and rare appearance in the scene. For changes in directional settings, sidewalks exhibited the most sensitivity.

Furthermore, there were differences across target features in how they responded to specific directions. The discrepancies between left and right, reported above, were found to be notably larger in roads and sidewalks compared with other target features. With 20-meter intervals, FBLR-FB pairs had a higher correlation than any other directional settings in the cases of objects, sky, and vegetation (Table 3). However, the other feature categories showed a relatively higher correlation with FBLR-LR. These (feature-specific) distinct patterns can also be seen in Appendix C where we explored how the correlations responded to various parameter setting changes.

### *4.3. Local variation patterns*

As noted in the preceding section, this study attempted to examine local variation patterns – i.e., where GSV measures are likely to vary more widely – as well as the global sensitivity discussed above. This was accomplished by estimating a set of multivariate regression models in a

standardized fashion as explained in section 3, and the results are summarized in Table 5 where only significant results are reported for brevity.

<< Insert Table 5 about here >>

As shown in the table, *segment.length* consistently had a significant negative influence on the dependent variable – i.e., the absolute magnitude of the deviation from the baseline (which is 20m and FBLR) – as expected. Specifically, the deviation (due to a sparser spacing setting, such as 40m and 60m) tended to be smaller on longer street segments for all nine target features. For many target features, *segment.length* was also found to mitigate the absolute magnitude of the deviation due to changes in directional setting. However, such a significant negative impact was not detected in the cases of buildings and roads, suggesting that the degree of their measurement sensitivity to direction was not necessarily lower on longer street segments.

Additionally, *z-baseline(itself)* – e.g., $z(p_{20m,FBLR}^{Humans})$ as a determinant of the deviation in humans measurement outcomes – was found to matter in many target feature categories. With respect to spacing, in all but roads and sky, it was positively associated with the dependent variable, suggesting that the deviation tended to be larger where the target feature was relatively abundant. This makes sense because no deviation would arise due to sparse spacing if the target feature did not exist at all on the street segment. Roads and sky are somewhat ubiquitous, so such a significant positive association would not be expected in these categories, again highlighting one of the important findings of this study that the measurement sensitivity is feature-dependent.

*z-baseline(itself)* also appeared to matter in understanding the deviation caused by directional setting changes. Again, in many categories, it was positively related to the dependent variable. Sky, however, showed a negative association between *z-baseline(Sky)* and the

magnitude of the deviation due to a narrower directional coverage. This finding implies that sky measures had little variability in low-density areas and/or widely open locations where it accounted for a large proportion of the GSV image pixels. Rather, the sky measurement outcomes tended to vary more widely in high-density districts in the city having fewer sky pixels in the street view images.

Regarding the local variation, there are a few additional notable patterns that seem to be associated with the ways in which multiple target features are combined or separated spatially. For instance, *z-baseline(Objects),* as well as the abundance of roads and sidewalks, was often found to have a significant, positive relationship with the deviation in building measurement outcomes, indicating that the variation in GSV-based building metrics can increase in areas with a higher percentage of these features rather than sky or vegetation. At the same time, in some settings, *z-baseline(Buildings)* showed a negative relationship with the deviation in sidewalks. The bidirectional association between buildings and sidewalks reveals the tendency for them to locate together and make up the local streetscape in a concerted fashion, and such connections may deserve attention, as they enable researchers to refine urban landscape measurement strategies.

## 5. Summary and Discussion

Over the last few decades, new data opportunities have emerged for scholars who seek to better measure the physical environment of our cities as a manifestation of the history and culture of their inhabitants or as a key factor that shapes the way we live in the urban environment. Street view imagery has been recognized as one of the more promising sources of such data, and

researchers have started to take advantage of this new data opportunity. However, little guidance is available on how to use the imagery for measuring diverse urban landscapes effectively. Furthermore, there is a dearth of research on how measurement outcomes may vary depending on the way street view imagery is used.

In this context, this study explored ways to derive street-level measures of the physical environment using GSV images and examined the extent to which these measures are influenced by the data acquisition/processing parameter settings. Explicit consideration was given to spacing, directions, and target features for which no systematic investigations are currently available in the literature. More specifically, in this study, we empirically assessed both the global sensitivity and local variation patterns using data for street segments in the City of Santa Ana to inform future research and relevant practice.

Above all, our assessment results clearly showed that the GSV measures could vary substantially depending on the parameter setting used. Using midpoints or long intervals was found to lead to higher variability. Such spacing can also affect the measurement outcomes of street segments with varying lengths differently. Therefore, researchers should be cautious in using sparse spacing, particularly if they seek to capture subtle micro-level changes in the built environment. Similarly, narrower directional settings can prevent one from capturing the surrounding physical environment precisely. In other words, both the spatial scale and extent matter, as they do in other data, metrics, and processes (see e.g., Turner et al., 1989; Atkinson and Tate, 2000; Kim, 2013; Labib et al., 2020).

The level of sensitivity, however, differs significantly by target feature, as summarized in Table 6. While some common features, such as sky and vegetation, appeared to be less sensitive to changes in spacing and/or directional settings, the proportion of human and object pixels

captured in GSV images varied much more substantially. This finding is in line with those of some previous studies suggesting that challenges exist in detecting small or transient features using GSV (Bader et al., 2015 and 2017; Nesse and Airt, 2020). In Santa Ana, sidewalks also showed a high level of (global) sensitivity, particularly with respect to directions, requiring caution in determining the associated parameter setting for GSV acquisition. With the caveat that there may be differences in our study area compared to other potential study sites, the last column of Table 6 uses the information from Appendix C to offer guidance on whether it is more reliable to use fewer images based on longer intervals, only left-right images, or only front-back images. [4]

<< Insert Table 6 about here >>

The global sensitivity assessment results also highlighted the asymmetric nature of urban landscapes. Left and right-side street images often yielded a very different composition of the streetscape, whereas a relatively higher level of consistency was detected between front and back images. Again. such a wide left-right discrepancy tends to be larger in the cases of some target features, such as roads and sidewalks. Perhaps, this is in part due to the way in which our study area (Santa Ana) has been designed and developed, but many American cities are likely to share similar characteristics of the built environment, and the asymmetry deserves attention in gathering and processing GSV images for urban research purposes.

[4] For buildings, roads, and sidewalks, it is better to use longer intervals (but all four images at each location) if one wishes to restrict the sample of images (Note: for these features, the reliability reduction shown in Appendix C is lower for collecting images every 40 meters, compared to using just front+back or left+right images). Humans are the only feature in which it is better to focus on left+right images (but with short intervals), which may be due to their more likely presence on sidewalks. And for the other features – objects, sky, terrain, vegetation, and vehicles – it seems better to focus on front+back images (with short intervals) if one wishes to limit the sample size. Nonetheless, objects are so rare that any approach limiting the number of images can greatly reduce the reliability of this measure.

Most likely the measures do not respond to changes in parameter settings in a spatially uniform fashion. That is, in some parts of a city (or some types of street segments), researchers should expect a higher degree of variability, while that will not be the case in other locations; and again, the local variation pattern differs across target features. However, variability was less of a problem on longer street segments given that they provide the researcher with more data acquisition points even with a sparser spacing option (unless a simple midpoint data acquisition strategy is adopted). Furthermore, the local variation pattern was associated with the ways in which various elements of the streetscape co-occurred. The variability of sidewalks, for instance, was tightly linked to the presence of buildings. This finding suggests that there is an opportunity for researchers to better handle the sensitivity issues using their knowledge about the built environment in their study areas. In the case of Santa Ana, one could attempt to gather both sidewalk and building information and combine the two (or quantify the degree of divergence between the two) to better capture the nuanced complexity of the city's streetscapes.

It should be stressed that strategies for using GSV will differ from one study to another, and the data collection and measurement strategies must reflect the research questions (and underlying theories) examined in each project. Furthermore, the findings drawn from Santa Ana will not necessarily hold true in other urban settings, although the city was used in this study given its ability to represent diverse urban physical settings. Likewise, our findings using GSV may not readily apply to other sources/platforms of urban street imagery information. It also needs to be acknowledged that the present assessment did not address other parameters of the GSV extraction that could be varied and also be important, including the point-of-view, pitch, and temporal settings.

Nevertheless, what is presented in this article strongly suggests that we should not underestimate (or deflect attention away from) the importance of GSV data acquisition and processing settings. Rather, we should make them more transparent and generate relevant guidance for more effective and cautious use of GSV, which was the main objective of this study. Building on the findings of the present study, future research may examine the variability of GSV measures in other contexts and its impacts on study findings. This line of research can further be integrated with the development (or improvement) of street imagery data platforms and computer vision technologies for image processing.

**References**


Anguelov, D., Dulong, C., Filip, D., Frueh, C., Lafon, S., Lyon, R., ... & Weaver, J. (2010). Google street view: Capturing the world at street level. *Computer*, 43(6), 32-38.

Atkinson, P. M., & Tate, N. J. (2000). Spatial scale problems and geostatistical solutions: a review. *The Professional Geographer*, 52(4), 607-623.

Bader, M. D., Mooney, S. J., Lee, Y. J., Sheehan, D., Neckerman, K. M., Rundle, A. G., & Teitler, J. O. (2015). Development and deployment of the Computer Assisted Neighborhood Visual Assessment System (CANVAS) to measure health-related neighborhood conditions. *Health & Place*, 31, 163-172.

Bader, M. D., Mooney, S. J., Bennett, B., & Rundle, A. G. (2017). The promise, practicalities, and perils of virtually auditing neighborhoods using Google street view. *The Annals of the American Academy of Political and Social Science*, 669(1), 18-40.

Barbierato, E., Bernetti, I., Capecchi, I., & Saragosa, C. (2020). Integrating remote sensing and street view images to quantify urban forest ecosystem services. *Remote Sensing*, 12(2), 329.

Campbell, A., Both, A., & Sun, Q. C. (2019). Detecting and mapping traffic signs from Google Street View images using deep learning and GIS. *Computers, Environment and Urban Systems*, 77, 101350.

Chen, L. C., Papandreou, G., Schroff, F., & Adam, H. (2017). Rethinking atrous convolution for semantic image segmentation. arXiv:1706.05587.

Chen, L. C., Zhu, Y., Papandreou, G., Schroff, F., & Adam, H. (2018). Encoder-decoder with atrous separable convolution for semantic image segmentation. In Proceedings of the European Conference on Computer Vision (pp. 801-818).

Cordts, M., Omran M., Ramos, S., Rehfeld, T., Enzweiler, M., Benenson, R., … & Schiele, B. (2016). The cityscapes dataset for semantic urban scene understanding. Paper read at Proceedings of the IEEE Conference on Computer Vision and Pattern Recognition.

Curtis, A., Duval-Diop, D., & Novak, J. (2010). Identifying spatial patterns of recovery and abandonment in the post-Katrina Holy Cross neighborhood of New Orleans. *Cartography and Geographic Information Science*, 37(1), 45-56.

Egli, V., Zinn, C., Mackay, L., Donnellan, N., Villanueva, K., Mavoa, S., ... & Smith, M. (2019). Viewing obesogenic advertising in children's neighbourhoods using Google Street View. *Geographical Research*, 57(1), 84-97.

Gebru, T., Krause, J., Wang, Y., Chen, D., Deng, J., Aiden, E. L., & Fei-Fei, L. (2017). Using deep learning and Google Street View to estimate the demographic makeup of neighborhoods across the United States. *Proceedings of the National Academy of Science*s, 114(50), 13108-13113.

Gobster, P. H., Hadavi, S., Rigolon, A., & Stewart, W. P. (2020). Measuring landscape change, lot by lot: Greening activity in response to a vacant land reuse program. *Landscape and Urban Planning*, 196, 103729.

Goel, R., Garcia, L. M., Goodman, A., Johnson, R., Aldred, R., Murugesan, M., ... & Woodcock, J. (2018). Estimating city-level travel patterns using street imagery: A case study of using Google Street View in Britain. *PloS One*, 13(5), e0196521.

Gong, F. Y., Zeng, Z. C., Zhang, F., Li, X., Ng, E., & Norford, L. K. (2018). Mapping sky, tree, and building view factors of street canyons in a high-density urban environment. *Building and Environment*, 134, 155-167.

Guo, Z. (2013). Residential street parking and car ownership: A study of households with off-street parking in the New York City region. *Journal of the American Planning Association*, 79(1), 32-48.

He, L., Páez, A., & Liu, D. (2017). Built environment and violent crime: An environmental audit approach using Google Street View. *Computers, Environment and Urban Systems*, 66, 83-95.

Hwang, J., & Sampson, R. J. (2014). Divergent pathways of gentrification: Racial inequality and the social order of renewal in Chicago neighborhoods. *American Sociological Review*, 79(4), 726-751.

Kim, J. H. (2013). Spatiotemporal scale dependency and other sensitivities in dynamic land-use change simulations. *International Journal of Geographical Information Science*, 27(9), 1782-1803.

Labib, S. M., Lindley, S., & Huck, J. J. (2020). Scale effects in remotely sensed greenspace metrics and how to mitigate them for environmental health exposure assessment. *Computers, Environment and Urban Systems*, 82, 101501.

Law, S., Seresinhe, C. I., Shen, Y., & Gutierrez-Roig, M. (2020). Street-Frontage-Net: Urban image classification using deep convolutional neural networks. *International Journal of Geographical Information Science*, 34(4), 681-707.

Lee, S., & Talen, E. (2014). Measuring walkability: A note on auditing methods. *Journal of Urban Design*, 19(3), 368-388.

Leon, L. F. A., & Quinn, S. (2019). The value of crowdsourced street-level imagery: Examining the shifting property regimes of OpenStreetCam and Mapillary. *GeoJournal*, 84(2), 395-414.

Li, X., Santi, P., Courtney, T. K., Verma, S. K., & Ratti, C. (2018). Investigating the association between streetscapes and human walking activities using Google Street View and human trajectory data. *Transactions in GIS*, 22(4), 1029-1044.

Li, X., & Ratti, C. (2019). Mapping the spatio-temporal distribution of solar radiation within street canyons of Boston using Google Street View panoramas and building height model. *Landscape and Urban Planning*, 191, 103387.

Li, X., Duarte, F., & Ratti, C. (2019). Analyzing the obstruction effects of obstacles on light pollution caused by street lighting system in Cambridge, Massachusetts. *Environment and Planning B: Urban Analytics and City Science*, 2399808319861645.

Lu, Y., Sarkar, C., & Xiao, Y. (2018). The effect of street-level greenery on walking behavior: Evidence from Hong Kong. *Social Science & Medicine*, 208, 41-49.

Lu, Y. (2019). Using Google Street View to investigate the association between street greenery and physical activity. *Landscape and Urban Planning*, 191, 103435.

Lu, Y., Yang, Y., Sun, G., & Gou, Z. (2019). Associations between overhead-view and eye-level urban greenness and cycling behaviors. *Cities*, 88, 10-18.

Middel, A., Lukasczyk, J., Zakrzewski, S., Arnold, M., & Maciejewski, R. (2019). Urban form and composition of street canyons: A human-centric big data and deep learning approach. *Landscape and Urban Planning*, 183, 122-132.

Nesse, K., & Airt, L. (2020). Google Street View as a replacement for in-person street surveys: Meta-analysis of findings from evaluations. *Journal of Urban Planning and Development*, 146(2), 04020013.

Nguyen, Q. C., Khanna, S., Dwivedi, P., Huang, D., Huang, Y., Tasdizen, T., ... & Jiang, C. (2019). Using Google Street View to examine associations between built environment characteristics and US health outcomes. *Preventive Medicine Reports*, 14, 100859.

Salesses, P., Schechtner, K., & Hidalgo, C. A. (2013). The collaborative image of the city: Mapping the inequality of urban perception. *PloS One*, 8(7), e68400.

Seiferling, I., Naik, N., Ratti, C., & Proulx, R. (2017). Green streets − Quantifying and mapping urban trees with street-level imagery and computer vision. *Landscape and Urban Planning*, 165, 93-101.

Turner, M. G., O'Neill, R. V., Gardner, R. H., & Milne, B. T. (1989). Effects of changing spatial scale on the analysis of landscape pattern. *Landscape Ecology*, 3(3), 153-162.

Wang, M., & Vermeulen, F. (2020). Life between buildings from a street view image: What do big data analytics reveal about neighbourhood organisational vitality? *Urban Studies*, 0042098020957198.

Yang, Y., He, D., Gou, Z., Wang, R., Liu, Y., & Lu, Y. (2019). Association between street greenery and walking behavior in older adults in Hong Kong. *Sustainable Cities and Society*, 51, 101747.

Ye, Y., Richards, D., Lu, Y., Song, X., Zhuang, Y., Zeng, W., & Zhong, T. (2019). Measuring daily accessed street greenery: A human-scale approach for informing better urban planning practices. *Landscape and Urban Planning*, 191, 103434.

Yin, L., Cheng, Q., Wang, Z., & Shao, Z. (2015). 'Big data' for pedestrian volume: Exploring the use of Google Street View images for pedestrian counts. *Applied Geography*, 63, 337-345.

**Table 1. Summary of a sample of large-scale GSV applications**

| Author(s) | Publication year | Topic(s) | Study region(s) | GSV acquisition settings | |
|---|---|---|---|---|---|
| | | | | Spacing | Direction(s) |
| Seiferling et al. | 2017 | Street greenery | New York and Boston | 15 meters | East (90 degree) |
| Gong et al. | 2018 | Sky, tree, and building views | Hong Kong | 30 meters | GSV Panoramas |
| Li et al. | 2018 | Street greenery | Boston | 100 meters | Panoramas (and more) |
| Lu et al. | 2018 | Street greenery | Hong Kong | 50 meters | North, East, South, West |
| Li & Ratti | 2019 | Solar radiation | Boston | 100 meters | GSV Panoramas |
| Lu | 2019 | Street greenery | Hong Kong | 20 meters | North, East, South, West |
| Lu et al. | 2019 | Street greenery | Hong Kong | 50 meters | North, East, South, West |
| Ye et al. | 2019 | Street greenery | Singapore | 50 meters | Front, Back, Left, Right |
| Yang et al. | 2019 | Street greenery | Hong Kong | 50 meters | North, East, South, West |
| Law et al. | 2020 | Street frontage quality | London | Midpoints | Front |

Note: Li et al. (2018) also used six horizontal static images to calculate the Green View Index.

**Table 2. Correlations between 20-meter intervals and alternative spacing schemes (all four directions)**

| Comparisons | Mean | Buildings | Humans | Objects | Roads | Sidewalks | Sky | Terrain | Vegetation | Vehicles |
|---|---|---|---|---|---|---|---|---|---|---|
| 20m-40m | 0.951 | 0.984 | 0.837 | 0.937 | 0.957 | 0.954 | 0.981 | 0.981 | 0.981 | 0.946 |
| 20m-60m | 0.888 | 0.955 | 0.665 | 0.862 | 0.908 | 0.887 | 0.949 | 0.945 | 0.951 | 0.868 |
| 20m-80m | 0.852 | 0.928 | 0.614 | 0.824 | 0.877 | 0.846 | 0.915 | 0.912 | 0.917 | 0.836 |
| 20m-100m | 0.805 | 0.883 | 0.539 | 0.780 | 0.833 | 0.802 | 0.882 | 0.888 | 0.885 | 0.755 |
| 20m-midpoints | 0.777 | 0.883 | 0.488 | 0.733 | 0.801 | 0.749 | 0.873 | 0.854 | 0.875 | 0.733 |
| % (in all GSV images) | | 5.9% | 0.1% | 0.4% | 27.9% | 3.0% | 34.2% | 2.4% | 22.0% | 4.3% |

Note: See Appendix A for the correlation patterns when other directional settings were adopted.

**Table 3. Correlations between all four directions and alternative directional settings (20-meter intervals)**

| Comparisons | Mean | Buildings | Humans | Objects | Roads | Sidewalks | Sky | Terrain | Vegetation | Vehicles |
|---|---|---|---|---|---|---|---|---|---|---|
| FBLR-FB | 0.928 | 0.960 | 0.844 | 0.932 | 0.878 | 0.854 | 0.981 | 0.969 | 0.982 | 0.949 |
| FBLR-LR | 0.960 | 0.989 | 0.922 | 0.921 | 0.973 | 0.901 | 0.976 | 0.991 | 0.980 | 0.984 |
| FBLR-Front | 0.867 | 0.918 | 0.652 | 0.866 | 0.802 | 0.820 | 0.958 | 0.932 | 0.960 | 0.898 |
| FBLR-Back | 0.880 | 0.934 | 0.713 | 0.872 | 0.809 | 0.825 | 0.961 | 0.937 | 0.962 | 0.903 |
| FBLR-Left | 0.760 | 0.809 | 0.708 | 0.717 | 0.694 | 0.592 | 0.825 | 0.808 | 0.857 | 0.831 |
| FBLR-Right | 0.750 | 0.775 | 0.647 | 0.716 | 0.709 | 0.593 | 0.822 | 0.811 | 0.846 | 0.834 |

Note: See Appendix B for the correlation patterns when other spacing schemes were adopted.

**Table 4. Correlations between Left and Right sides (compared with the Front-Back correlations)**

| Comparison setting | | Mean | Buildings | Humans | Objects | Roads | Sidewalks | Sky | Terrain | Vegetation | Vehicles |
|---|---|---|---|---|---|---|---|---|---|---|---|
| 20m | Left-Right | 0.243 | 0.283 | 0.085 | 0.212 | 0.039 | -0.135 | 0.424 | 0.335 | 0.510 | 0.431 |
| | Front-Back | 0.770 | 0.860 | 0.308 | 0.737 | 0.685 | 0.856 | 0.912 | 0.860 | 0.914 | 0.801 |
| 40m | Left-Right | 0.202 | 0.269 | 0.030 | 0.162 | 0.032 | -0.111 | 0.363 | 0.304 | 0.427 | 0.346 |
| | Front-Back | 0.649 | 0.771 | 0.118 | 0.557 | 0.598 | 0.735 | 0.818 | 0.772 | 0.827 | 0.641 |
| 60m | Left-Right | 0.185 | 0.225 | 0.034 | 0.112 | 0.089 | -0.072 | 0.340 | 0.271 | 0.400 | 0.271 |
| | Front-Back | 0.540 | 0.658 | 0.060 | 0.364 | 0.490 | 0.651 | 0.722 | 0.700 | 0.723 | 0.493 |
| 80m | Left-Right | 0.144 | 0.233 | 0.010 | 0.053 | 0.044 | -0.082 | 0.253 | 0.237 | 0.299 | 0.246 |
| | Front-Back | 0.502 | 0.640 | 0.030 | 0.321 | 0.477 | 0.606 | 0.678 | 0.645 | 0.686 | 0.432 |
| 100m | Left-Right | 0.139 | 0.177 | -0.013 | 0.085 | 0.039 | -0.081 | 0.269 | 0.226 | 0.329 | 0.220 |
| | Front-Back | 0.450 | 0.540 | 0.104 | 0.297 | 0.355 | 0.527 | 0.619 | 0.578 | 0.629 | 0.404 |
| Mid-points | Left-Right | 0.115 | 0.182 | 0.017 | 0.002 | 0.045 | -0.095 | 0.243 | 0.201 | 0.278 | 0.163 |
| | Front-Back | 0.437 | 0.512 | 0.066 | 0.189 | 0.424 | 0.533 | 0.614 | 0.596 | 0.613 | 0.381 |

**Table 5. Regression analysis results: Segment-level determinants of the deviation from the baseline (20m and FBLR)**

| Variable | Buildings | Humans | Objects | Roads | Sidewalks | Sky | Terrain | Vegetation | Vehicles |
|---|---|---|---|---|---|---|---|---|---|
| **when using 40m and FBLR** | | | | | | | | | |
| segment.length (in km) | -0.303 | -0.719 | -0.500 | -0.605 | -0.541 | -0.398 | -0.354 | -0.403 | -0.556 |
| z-baseline(Buildings) | 0.055 | 0.042 | | | | | 0.013 | | |
| z-baseline(Humans) | | 0.327 | 0.011 | | | | | -0.006 | |
| z-baseline(Objects) | 0.007 | | 0.121 | | | -0.009 | | | |
| z-baseline(Roads) | 0.010 | 0.036 | | -0.029 | | | | | -0.017 |
| z-baseline(Sidewalks) | 0.008 | | | -0.013 | 0.057 | | | 0.007 | |
| z-baseline(Sky) | | 0.111 | | | | | 0.055 | | |
| z-baseline(Terrain) | | 0.032 | | | | | 0.061 | | |
| z-baseline(Vegetation) | | 0.113 | | | | | 0.062 | | *excluded* |
| z-baseline(Vehicles) | *excluded* | *excluded* | *excluded* | *excluded* | *excluded* | *excluded* | *excluded* | *excluded* | 0.066 |
| **when using 60m and FBLR** | | | | | | | | | |
| segment.length (in km) | -0.528 | -0.775 | -0.901 | -0.825 | -0.902 | -0.643 | -0.639 | -0.653 | -0.806 |
| z-baseline(Buildings) | 0.067 | | | | | | 0.025 | | |
| z-baseline(Humans) | 0.012 | 0.462 | 0.016 | | | | 0.011 | | |
| z-baseline(Objects) | 0.016 | -0.033 | 0.178 | 0.019 | 0.028 | | | | |
| z-baseline(Roads) | | 0.039 | | -0.045 | -0.030 | | | | |
| z-baseline(Sidewalks) | | | 0.017 | -0.022 | 0.092 | | | | |
| z-baseline(Sky) | | | | -0.116 | | | 0.087 | | |
| z-baseline(Terrain) | | 0.058 | | -0.017 | -0.030 | | 0.116 | | |
| z-baseline(Vegetation) | | | | -0.119 | | | 0.090 | 0.083 | *excluded* |
| z-baseline(Vehicles) | *excluded* | *excluded* | *excluded* | *excluded* | *excluded* | *excluded* | *excluded* | *excluded* | 0.127 |
| **when using 20m and Front+Back** | | | | | | | | | |
| segment.length (in km) | | -0.635 | -0.372 | | -0.327 | -0.134 | -0.237 | -0.140 | -0.325 |
| z-baseline(Buildings) | 0.090 | | 0.034 | -0.035 | | 0.029 | | | |
| z-baseline(Humans) | | 0.282 | | | | | | | |
| z-baseline(Objects) | | | 0.137 | 0.030 | 0.030 | | | | |
| z-baseline(Roads) | 0.023 | | | | | 0.017 | | | |
| z-baseline(Sidewalks) | 0.013 | | | 0.080 | 0.161 | | 0.013 | | |
| z-baseline(Sky) | -0.064 | | | -0.214 | -0.119 | | | | |
| z-baseline(Terrain) | -0.013 | | | | | 0.010 | 0.071 | | |
| z-baseline(Vegetation) | | | 0.079 | -0.173 | -0.123 | | 0.055 | | *excluded* |
| z-baseline(Vehicles) | *excluded* | *excluded* | *excluded* | *excluded* | *excluded* | *excluded* | *excluded* | *excluded* | 0.080 |
| **when 20m and Left+Right** | | | | | | | | | |

| | | | | | | | | | |
|---|---|---|---|---|---|---|---|---|---|
| segment.length (in km) | | -0.352 | -0.375 | | | -0.131 | -0.118 | -0.138 | -0.157 |
| z-baseline(Buildings) | 0.039 | | | | | 0.030 | | | |
| z-baseline(Humans) | | 0.166 | | | | | | | |
| z-baseline(Objects) | | | 0.145 | 0.010 | 0.047 | | | | |
| z-baseline(Roads) | 0.010 | | | 0.016 | 0.020 | 0.018 | | | |
| z-baseline(Sidewalks) | 0.008 | | 0.017 | 0.035 | 0.150 | | 0.006 | | |
| z-baseline(Sky) | -0.052 | | | -0.061 | | -0.051 | | | |
| z-baseline(Terrain) | -0.006 | | | | | 0.011 | 0.035 | | |
| z-baseline(Vegetation) | -0.048 | | | | | | 0.031 | 0.047 | *excluded* |
| z-baseline(Vehicles) | *excluded* | *excluded* | *excluded* | *excluded* | *excluded* | *excluded* | *excluded* | *excluded* | 0.034 |
| **Frequencies of being significant in the remaining 37 settings** | | | | | | | | | |
| segment.length (in km) | 76% | 84% | 78% | 76% | 68% | 84% | 76% | 81% | 81% |
| z-baseline(Buildings) | 100% | 3% | 5% | 38% | 59% | 16% | 5% | 8% | 11% |
| z-baseline(Humans) | 38% | 95% | 16% | 24% | 3% | 27% | 3% | 22% | 8% |
| z-baseline(Objects) | 78% | 70% | 100% | 54% | 70% | 24% | 35% | 24% | 22% |
| z-baseline(Roads) | 78% | 32% | 11% | 51% | 30% | 24% | 5% | 16% | 35% |
| z-baseline(Sidewalks) | 59% | 49% | 27% | 51% | 100% | 49% | 70% | 38% | 8% |
| z-baseline(Sky) | 22% | 14% | 14% | 43% | 65% | 30% | 14% | 11% | 27% |
| z-baseline(Terrain) | 32% | 68% | 3% | 65% | 68% | 11% | 100% | 14% | 16% |
| z-baseline(Vegetation) | 16% | 11% | 5% | 43% | 65% | 3% | 19% | 46% | *excluded* |
| z-baseline(Vehicles) | *excluded* | *excluded* | *excluded* | *excluded* | *excluded* | *excluded* | *excluded* | *excluded* | 100% |

Note: For brevity, only significant estimates (at the 5% level) are presented in the table. To avoid singularity, z-baseline(Vehicles) was excluded from all models but those for Vehicles where z-baseline(Vegetation) was dropped instead of z-baseline(Vehicles).

**Table 6. Summary of findings**

| | | | | | |
|---|---|---|---|---|---|
| Overall | • A midpoint strategy (or sparse intervals) can lead to imprecise representation of streetscapes. Using sparse intervals is likely to perform worse on shorter street segments, though a midpoint approach may be worse for longer segments.<br>• One side's street view can be significantly different from those on other sides. Relying on the GSV images gathered with a narrow angle of view can result in biased estimates, although some researchers may intentionally focus on a certain side of the street view for their unique research questions or purposes.<br>• The sensitivity of GSV-based measures varies significantly by target feature. See below for the detailed patterns found in Santa Ana, California. The last column (based on Appendix C) shows which is the best strategy to use when limiting the number of images: Distance (better to choose longer intervals); LR (better to choose left and right images); FB (better to choose only front and back images). | | | | |
| | Features | Presence (frequency) | Sensitivity to spacing | Sensitivity to directions | Best tradeoff |
| Feature-specific | Buildings | Moderate | Low | Low | Distance |
| | Humans | Very small | High | High | LR |
| | Objects | Very small | Moderate | Moderate | FB |
| | Roads | Large | Moderate | Moderate | Distance |
| | Sidewalks | Small | Moderate | High | Distance |
| | Sky | Large | Low | Low | FB |
| | Terrain | Small | Low | Low | FB |
| | Vegetation | Large | Low | Low | FB |
| | Vehicles | Small | Moderate | Low | FB |

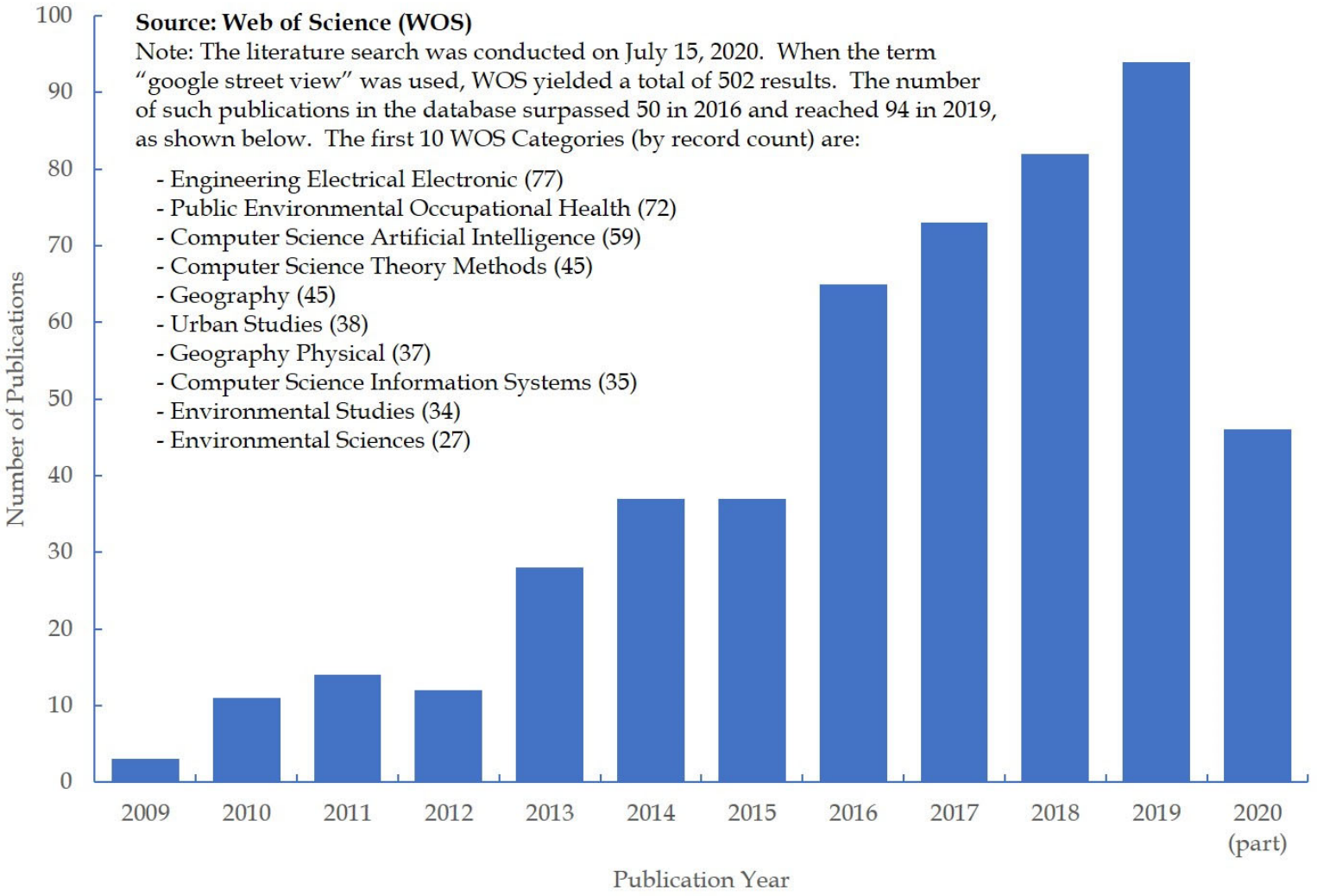


**Figure 1. Summary of the WOS search results**

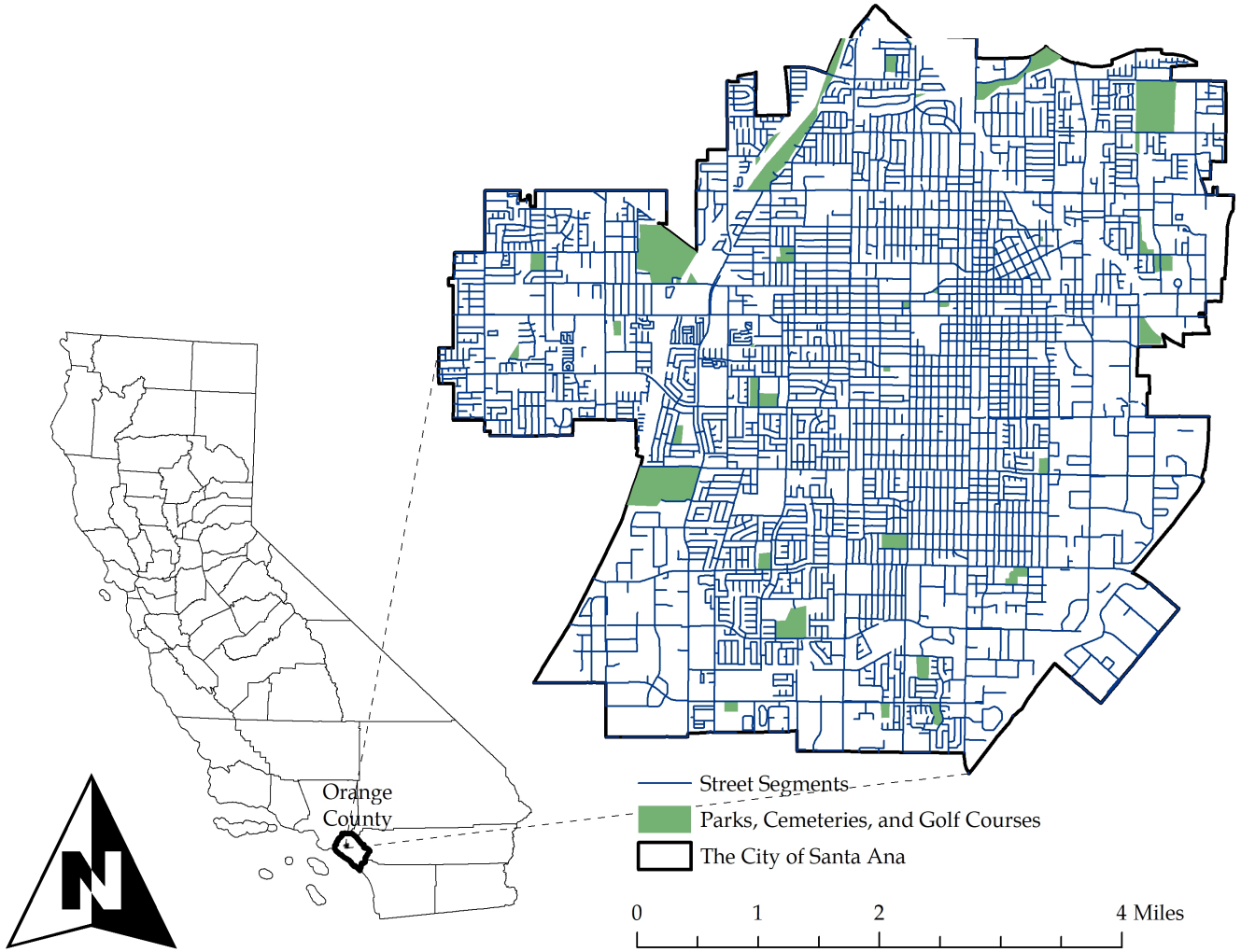


**Figure 2. Study area: Santa Ana, California**

**Major features:**
Roads 33.7%
Sky 32.4%
Buildings 26.8%
Sidewalks 3.9%
Vegetation 1.7%

**Major features:**
Vegetation 36.3%
Sky 21.6%
Vehicles 20.5%
Terrain 9.6%
Buildings 5.5%

**Major features:**
Sky 51.4%
Roads 32.8%
Buildings 10.1%
Vehicles 5.2%
Sidewalks 0.5%

Buildings
Humans
Objects
Roads
Sidewalks
Sky
Terrain
Vegetation
Vehicles

Note: Previous studies often processed the street view images solely based on RGB color band values, but this approach would not enable one to differentiate two distinct streetscape elements with the same color in the images effectively. We employed an advanced semantic segmentation technique (Deeplabv3+, Chen et al., 2018) that enabled us to overcome this limitation, as done in some recent studies, such as Barbierato et al. (2020) and Wang & Vermeulen (2020).

**Figure 3. Semantic segmentation examples**

## Appendix A. Sensitivity with respect to spacing

| Comparison setting | | Mean | Buildings | Humans | Objects | Roads | Sidewalks | Sky | Terrain | Vegetation | Vehicles |
|---|---|---|---|---|---|---|---|---|---|---|---|
| All directions (FBLR) | 20m-40m | 0.951 | 0.984 | 0.837 | 0.937 | 0.957 | 0.954 | 0.981 | 0.981 | 0.981 | 0.946 |
| | 20m-60m | 0.888 | 0.955 | 0.665 | 0.862 | 0.908 | 0.887 | 0.949 | 0.945 | 0.951 | 0.868 |
| | 20m-80m | 0.852 | 0.928 | 0.614 | 0.824 | 0.877 | 0.846 | 0.915 | 0.912 | 0.917 | 0.836 |
| | 20m-100m | 0.805 | 0.883 | 0.539 | 0.780 | 0.833 | 0.802 | 0.882 | 0.888 | 0.885 | 0.755 |
| | 20m-mid | 0.777 | 0.883 | 0.488 | 0.733 | 0.801 | 0.749 | 0.873 | 0.854 | 0.875 | 0.733 |
| Front+ Back | 20m-40m | 0.952 | 0.979 | 0.808 | 0.943 | 0.962 | 0.967 | 0.988 | 0.979 | 0.988 | 0.955 |
| | 20m-60m | 0.894 | 0.946 | 0.646 | 0.866 | 0.908 | 0.916 | 0.963 | 0.952 | 0.963 | 0.883 |
| | 20m-80m | 0.859 | 0.929 | 0.570 | 0.828 | 0.871 | 0.889 | 0.937 | 0.916 | 0.940 | 0.847 |
| | 20m-100m | 0.812 | 0.888 | 0.540 | 0.776 | 0.809 | 0.827 | 0.901 | 0.889 | 0.902 | 0.777 |
| | 20m-mid | 0.777 | 0.878 | 0.414 | 0.709 | 0.781 | 0.801 | 0.890 | 0.871 | 0.892 | 0.756 |
| Left+ Right | 20m-40m | 0.911 | 0.971 | 0.804 | 0.806 | 0.932 | 0.912 | 0.949 | 0.962 | 0.947 | 0.913 |
| | 20m-60m | 0.828 | 0.926 | 0.618 | 0.724 | 0.865 | 0.819 | 0.893 | 0.908 | 0.892 | 0.803 |
| | 20m-80m | 0.772 | 0.888 | 0.544 | 0.632 | 0.830 | 0.748 | 0.839 | 0.861 | 0.835 | 0.771 |
| | 20m-100m | 0.725 | 0.834 | 0.466 | 0.611 | 0.774 | 0.712 | 0.804 | 0.834 | 0.808 | 0.677 |
| | 20m-mid | 0.666 | 0.831 | 0.398 | 0.495 | 0.721 | 0.628 | 0.768 | 0.774 | 0.765 | 0.616 |
| Front | 20m-40m | 0.913 | 0.959 | 0.734 | 0.878 | 0.927 | 0.933 | 0.959 | 0.954 | 0.962 | 0.914 |
| | 20m-60m | 0.827 | 0.898 | 0.574 | 0.769 | 0.852 | 0.857 | 0.904 | 0.889 | 0.905 | 0.794 |
| | 20m-80m | 0.787 | 0.875 | 0.505 | 0.713 | 0.803 | 0.834 | 0.867 | 0.852 | 0.873 | 0.757 |
| | 20m-100m | 0.722 | 0.815 | 0.450 | 0.703 | 0.696 | 0.745 | 0.814 | 0.787 | 0.822 | 0.663 |
| | 20m-mid | 0.686 | 0.802 | 0.342 | 0.561 | 0.701 | 0.723 | 0.808 | 0.771 | 0.816 | 0.647 |
| Back | 20m-40m | 0.917 | 0.963 | 0.765 | 0.868 | 0.929 | 0.936 | 0.963 | 0.960 | 0.963 | 0.908 |
| | 20m-60m | 0.831 | 0.894 | 0.579 | 0.728 | 0.848 | 0.864 | 0.916 | 0.914 | 0.917 | 0.817 |
| | 20m-80m | 0.783 | 0.872 | 0.521 | 0.689 | 0.785 | 0.812 | 0.878 | 0.865 | 0.881 | 0.743 |
| | 20m-100m | 0.747 | 0.817 | 0.526 | 0.626 | 0.761 | 0.755 | 0.845 | 0.843 | 0.842 | 0.710 |
| | 20m-mid | 0.662 | 0.777 | 0.282 | 0.505 | 0.682 | 0.697 | 0.797 | 0.805 | 0.797 | 0.614 |
| Left | 20m-40m | 0.900 | 0.965 | 0.806 | 0.803 | 0.933 | 0.914 | 0.932 | 0.947 | 0.925 | 0.880 |
| | 20m-60m | 0.807 | 0.926 | 0.594 | 0.716 | 0.858 | 0.838 | 0.854 | 0.878 | 0.852 | 0.747 |
| | 20m-80m | 0.750 | 0.865 | 0.557 | 0.596 | 0.826 | 0.774 | 0.806 | 0.828 | 0.792 | 0.708 |
| | 20m-100m | 0.696 | 0.818 | 0.450 | 0.596 | 0.767 | 0.734 | 0.758 | 0.785 | 0.747 | 0.607 |
| | 20m-mid | 0.628 | 0.793 | 0.395 | 0.479 | 0.696 | 0.646 | 0.692 | 0.716 | 0.693 | 0.539 |
| Right | 20m-40m | 0.898 | 0.964 | 0.774 | 0.789 | 0.935 | 0.921 | 0.930 | 0.954 | 0.927 | 0.887 |
| | 20m-60m | 0.806 | 0.893 | 0.604 | 0.690 | 0.869 | 0.829 | 0.862 | 0.893 | 0.856 | 0.761 |
| | 20m-80m | 0.743 | 0.848 | 0.524 | 0.614 | 0.829 | 0.762 | 0.788 | 0.831 | 0.784 | 0.710 |
| | 20m-100m | 0.701 | 0.805 | 0.486 | 0.584 | 0.778 | 0.715 | 0.750 | 0.817 | 0.746 | 0.626 |
| | 20m-mid | 0.625 | 0.782 | 0.384 | 0.467 | 0.702 | 0.646 | 0.705 | 0.725 | 0.689 | 0.523 |

## Appendix B. Sensitivity with respect to directional settings

| Comparison setting | | Mean | Buildings | Humans | Objects | Roads | Sidewalks | Sky | Terrain | Vegetation | Vehicles |
|---|---|---|---|---|---|---|---|---|---|---|---|
| 20m | FBLR-FB | 0.928 | 0.960 | 0.844 | 0.932 | 0.878 | 0.854 | 0.981 | 0.969 | 0.982 | 0.949 |
| | FBLR-LR | 0.960 | 0.989 | 0.922 | 0.921 | 0.973 | 0.901 | 0.976 | 0.991 | 0.980 | 0.984 |
| | FBLR-F | 0.867 | 0.918 | 0.652 | 0.866 | 0.802 | 0.820 | 0.958 | 0.932 | 0.960 | 0.898 |
| | FBLR-B | 0.880 | 0.934 | 0.713 | 0.872 | 0.809 | 0.825 | 0.961 | 0.937 | 0.962 | 0.903 |
| | FBLR-L | 0.760 | 0.809 | 0.708 | 0.717 | 0.694 | 0.592 | 0.825 | 0.808 | 0.857 | 0.831 |
| | FBLR-R | 0.750 | 0.775 | 0.647 | 0.716 | 0.709 | 0.593 | 0.822 | 0.811 | 0.846 | 0.834 |
| 40m | FBLR-FB | 0.897 | 0.938 | 0.781 | 0.883 | 0.846 | 0.826 | 0.970 | 0.948 | 0.970 | 0.911 |
| | FBLR-LR | 0.948 | 0.985 | 0.909 | 0.885 | 0.968 | 0.896 | 0.964 | 0.985 | 0.966 | 0.975 |
| | FBLR-F | 0.806 | 0.867 | 0.512 | 0.786 | 0.756 | 0.775 | 0.921 | 0.887 | 0.924 | 0.827 |
| | FBLR-B | 0.825 | 0.898 | 0.652 | 0.771 | 0.757 | 0.763 | 0.929 | 0.898 | 0.929 | 0.825 |
| | FBLR-L | 0.743 | 0.808 | 0.735 | 0.683 | 0.683 | 0.582 | 0.794 | 0.793 | 0.818 | 0.794 |
| | FBLR-R | 0.724 | 0.759 | 0.556 | 0.665 | 0.706 | 0.613 | 0.798 | 0.797 | 0.815 | 0.806 |
| 60m | FBLR-FB | 0.865 | 0.915 | 0.758 | 0.824 | 0.795 | 0.792 | 0.958 | 0.925 | 0.956 | 0.861 |
| | FBLR-LR | 0.939 | 0.978 | 0.914 | 0.857 | 0.962 | 0.889 | 0.953 | 0.979 | 0.955 | 0.964 |
| | FBLR-F | 0.771 | 0.820 | 0.686 | 0.693 | 0.686 | 0.722 | 0.884 | 0.830 | 0.885 | 0.734 |
| | FBLR-B | 0.747 | 0.845 | 0.389 | 0.668 | 0.686 | 0.718 | 0.895 | 0.875 | 0.891 | 0.753 |
| | FBLR-L | 0.738 | 0.781 | 0.781 | 0.641 | 0.705 | 0.616 | 0.775 | 0.772 | 0.798 | 0.774 |
| | FBLR-R | 0.704 | 0.750 | 0.504 | 0.636 | 0.715 | 0.595 | 0.786 | 0.789 | 0.800 | 0.764 |
| 80m | FBLR-FB | 0.852 | 0.905 | 0.713 | 0.810 | 0.799 | 0.772 | 0.956 | 0.905 | 0.953 | 0.855 |
| | FBLR-LR | 0.933 | 0.978 | 0.891 | 0.840 | 0.960 | 0.887 | 0.951 | 0.975 | 0.952 | 0.966 |
| | FBLR-F | 0.740 | 0.816 | 0.462 | 0.677 | 0.686 | 0.704 | 0.874 | 0.820 | 0.874 | 0.743 |
| | FBLR-B | 0.740 | 0.823 | 0.557 | 0.638 | 0.687 | 0.680 | 0.877 | 0.822 | 0.876 | 0.703 |
| | FBLR-L | 0.712 | 0.782 | 0.715 | 0.594 | 0.679 | 0.592 | 0.755 | 0.772 | 0.771 | 0.749 |
| | FBLR-R | 0.698 | 0.753 | 0.539 | 0.625 | 0.708 | 0.610 | 0.750 | 0.761 | 0.763 | 0.775 |
| 100m | FBLR-FB | 0.836 | 0.892 | 0.731 | 0.755 | 0.758 | 0.759 | 0.950 | 0.896 | 0.948 | 0.839 |
| | FBLR-LR | 0.927 | 0.974 | 0.852 | 0.840 | 0.954 | 0.892 | 0.948 | 0.971 | 0.952 | 0.958 |
| | FBLR-F | 0.700 | 0.751 | 0.483 | 0.637 | 0.608 | 0.660 | 0.850 | 0.772 | 0.851 | 0.686 |
| | FBLR-B | 0.728 | 0.813 | 0.596 | 0.576 | 0.642 | 0.667 | 0.860 | 0.818 | 0.860 | 0.719 |
| | FBLR-L | 0.707 | 0.782 | 0.615 | 0.607 | 0.693 | 0.589 | 0.762 | 0.761 | 0.781 | 0.771 |
| | FBLR-R | 0.692 | 0.710 | 0.582 | 0.630 | 0.682 | 0.620 | 0.749 | 0.759 | 0.770 | 0.724 |
| mid | FBLR-FB | 0.821 | 0.893 | 0.675 | 0.732 | 0.756 | 0.766 | 0.942 | 0.888 | 0.937 | 0.800 |
| | FBLR-LR | 0.923 | 0.974 | 0.882 | 0.811 | 0.953 | 0.885 | 0.940 | 0.970 | 0.940 | 0.951 |
| | FBLR-F | 0.712 | 0.774 | 0.530 | 0.600 | 0.650 | 0.684 | 0.849 | 0.787 | 0.846 | 0.693 |
| | FBLR-B | 0.684 | 0.780 | 0.452 | 0.526 | 0.626 | 0.656 | 0.844 | 0.800 | 0.838 | 0.638 |
| | FBLR-L | 0.702 | 0.784 | 0.699 | 0.591 | 0.688 | 0.599 | 0.728 | 0.750 | 0.744 | 0.737 |
| | FBLR-R | 0.676 | 0.710 | 0.552 | 0.558 | 0.690 | 0.591 | 0.753 | 0.754 | 0.759 | 0.713 |

## Appendix C. Tradeoffs between spacing and directional settings

To gain a more nuanced understanding of the tradeoffs between the frequency of spacing and the number of images collected at each point, we estimated the marginal effect of a parameter setting change through multivariate regression. In this analysis, the outcome variable for each model is the correlation between a particular GSV acquisition strategy and the 20m-FBLR setting (baseline). The independent variables included binary variables indicating different spacing strategies (40m, 60m, 80m, 100m, and midpoints) and directional settings (front, back, left, right, FB, LR). We then estimated models for each of the nine target features and their average (i.e., the mean correlation across the nine categories). These variables explain between 96 and 99 percent of the variance in these models, indicating that they effectively uncover these relationships.

The model estimation results presented in the table below show how the correlations responded to the distinct parameter setting changes. In the first column, the -0.064 coefficient for "40-meter" indicates that collecting all 4 images every 40 meters (instead of every 20 meters) is expected to reduce the correlation by 0.064 on average. Collecting them every 60 meters is expected to reduce the correlation 0.132, every 80 meters reduces it 0.171, every 100 meters reduces it 0.218, and using the midpoint strategy reduces it 0.245. Or, if we were to collect images every 20 meters, but only collect images from the front, the correlation is reduced 0.152; if we only collect them from the back, the outcome variable is reduced 0.136, whereas collecting them from only the left or only the right reduces it much more (0.266 and 0.278).

As another way to think about these tradeoffs, we can consider the number of images collected as a "cost." In this case, a segment in which there are eight locations each 20 meters apart would require 32 images (4 front/back/left/right at each of 8 locations). There are different ways to collect only 16 images on this segment: (1) collecting them every 40 meters apart would be expected to require 16 images (4 at each of 4 locations); (2-3) collecting them every 20 meters but just 2 images at each point (either front+back or left+right – i.e., 2 images at each of 8 locations). In general, collecting 4 images with sparser spacing appears to induce a smaller reduction in correlation than comparable strategies with left and right directions only – for example, the overall correlation reduction is approximately -0.064 every 40 meters vs. -0.090 for left+right images, although this is not the case for the following two categories: Humans and Vehicles.

There are different ways to collect 8 images on this segment: (1) collecting them every 80 meters (4 at each of 2 locations); (2-5) collecting just one image every 20 meters (either front, back, left, or right – i.e., 1 image at each of 8 locations). The results suggest that using just the left or the right images can lead to a significant correlation reduction. It should be stressed, however, that the marginal effect of a certain parameter setting change varies across target features. Furthermore, as mentioned throughout the paper, the GSV acquisition parameter setting should reflect the objectives and design of each research project.

**Appendix C (Continued.)**

| Indicator variables | Regression models | | | | | | | | | |
|---|---|---|---|---|---|---|---|---|---|---|
| | Mean | Buildings | Humans | Objects | Roads | Sidewalks | Sky | Terrain | Vegetation | Vehicles |
| 40-meter | -0.064 ** | -0.027 ** | -0.162 ** | -0.099 ** | -0.048 ** | -0.049 ** | -0.039 ** | -0.032 ** | -0.041 ** | -0.076 ** |
| 60-meter | -0.132 ** | -0.074 ** | -0.289 ** | -0.200 ** | -0.099 ** | -0.111 ** | -0.084 ** | -0.078 ** | -0.087 ** | -0.171 ** |
| 80-meter | -0.171 ** | -0.095 ** | -0.349 ** | -0.245 ** | -0.131 ** | -0.148 ** | -0.125 ** | -0.118 ** | -0.129 ** | -0.204 ** |
| 100-meter | -0.218 ** | -0.150 ** | -0.406 ** | -0.287 ** | -0.185 ** | -0.185 ** | -0.160 ** | -0.150 ** | -0.160 ** | -0.279 ** |
| midpoints | -0.245 ** | -0.150 ** | -0.444 ** | -0.346 ** | -0.198 ** | -0.226 ** | -0.175 ** | -0.176 ** | -0.180 ** | -0.306 ** |
| Front | -0.152 ** | -0.126 ** | -0.281 ** | -0.174 ** | -0.222 ** | -0.170 ** | -0.079 ** | -0.108 ** | -0.076 ** | -0.135 ** |
| Back | -0.136 ** | -0.096 ** | -0.245 ** | -0.188 ** | -0.197 ** | -0.173 ** | -0.059 ** | -0.079 ** | -0.059 ** | -0.125 ** |
| Left | -0.266 ** | -0.209 ** | -0.240 ** | -0.355 ** | -0.300 ** | -0.382 ** | -0.238 ** | -0.232 ** | -0.218 ** | -0.224 ** |
| Right | -0.278 ** | -0.262 ** | -0.287 ** | -0.371 ** | -0.287 ** | -0.390 ** | -0.235 ** | -0.222 ** | -0.223 ** | -0.224 ** |
| FB | -0.053 ** | -0.032 ** | -0.122 ** | -0.056 ** | -0.107 ** | -0.103 ** | -0.004 | -0.021 * | -0.003 | -0.027 |
| LR | -0.090 ** | -0.042 ** | -0.097 ** | -0.197 ** | -0.064 ** | -0.148 ** | -0.076 ** | -0.046 ** | -0.075 ** | -0.069 ** |
| Intercept | 1.017 ** | 1.022 ** | 0.965 ** | 1.052 ** | 1.006 ** | 0.993 ** | 1.031 ** | 1.022 ** | 1.034 ** | 1.029 ** |
| Adj. R-squared | 0.987 | 0.974 | 0.974 | 0.977 | 0.982 | 0.982 | 0.970 | 0.979 | 0.961 | 0.971 |

** Significant at 1% level. * Significant at 5% level.